

This work has been submitted to IFAC for possible publication

# Trajectory Optimization by Successive Pseudospectral Convexification on Riemannian Manifolds

Tatsuya Narumi \* Shin-ichiro Sakai \*\*

\* Department of Advanced Energy, The University of Tokyo, Chiba, Japan (e-mail: [narumi.tatsuya24@ae.k.u-tokyo.ac.jp](mailto:narumi.tatsuya24@ae.k.u-tokyo.ac.jp)).

\*\* JAXA Institute of Space and Astronautical Science, Kanagawa, Japan (e-mail: [sakai@isas.jaxa.jp](mailto:sakai@isas.jaxa.jp)).

**Abstract:** This paper proposes an intrinsic pseudospectral convexification framework for optimal control problems with manifold constraints. While successive pseudospectral convexification combines spectral collocation with successive convexification, classical pseudospectral methods are not geometry-consistent on manifolds. This is because interpolation and differentiation are performed in Euclidean coordinates. We introduce a geometry-consistent transcription that enables pseudospectral collocation without imposing manifold constraints extrinsically. The resulting method solves nonconvex manifold-constrained problems through a sequence of convex subproblems. A six-degree-of-freedom landing guidance example with unit quaternions and unit thrust-direction vectors demonstrates the practicality of the approach and preserves manifold feasibility to machine precision.

**Keywords:** Intrinsic successive convexification, Pseudospectral method, Optimal control on Riemannian manifolds, Manifold-constrained trajectory optimization, Landing guidance.

## 1. INTRODUCTION

A central challenge in trajectory optimization is to faithfully represent the complex, nonconvex nature of physical systems within a computationally tractable framework. To address this challenge, Successive Convexification (SCvx) by Mao et al. (2016), has emerged as a predominant direct optimization approach. This framework iteratively solves convex approximations of the original nonconvex problem, constructed by linearizing dynamics and constraints around a reference trajectory. Owing to its tractability and favorable convergence properties, SCvx has become a standard tool in guidance and control. Recently, its scope has been expanded to handle even logical complexity; for instance, Szmuk et al. (2020), demonstrated that if/then constraints can be effectively incorporated within the SCvx framework.

Despite this progress in SCvx, the treatment of *geometric* complexity—specifically, nonlinear manifold constraints such as the quaternion unit-norm constraint  $\|q\| = 1$ —remains neglected (e.g., Szmuk and Açıkmese (2018)) or extrinsic. Existing extrinsic approaches, such as Lu (2021) and Sagliano et al. (2024), embed the manifold in Euclidean space as a nonlinear equality  $h(x) = 0$ . However, this extrinsic strategy does not strictly respect the manifold structure and incurs computational overhead, typically requiring additional constraints or variables for a single scalar constraint. Crucially, its applicability is fundamentally limited to manifolds defined by  $h(x) = 0$ , where  $h$  is a convex function.

Intrinsic methods, in contrast, preserve the geometry explicitly through operations on tangent spaces and retractions. In particular, Kraisler et al. (2025) proposed an intrinsic SCvx framework that avoids reliance on a specific Euclidean embedding and supports a wide range of Riemannian manifolds via retraction-based local parameterizations. However, this intrinsic formulation is discrete-time (e.g.,  $x_{k+1} = f(x_k, u_k)$ ) and therefore does not directly interface with pseudospectral transcriptions Sagliano et al. (2021), where global interpolation and differentiation enable *spectral convergence* (i.e., high accuracy with few nodes). This gap prevents combining intrinsic SCvx with the numerical efficiency of spectral collocation.

Motivated by tangent-space collocation formulations for direct methods Bordalba et al. (2023) and Lie group optimization Saccon et al. (2013), we develop an intrinsic successive pseudospectral convexification framework for manifold-constrained optimal control. The main contributions of this paper are

- We propose an *intrinsic pseudospectral method* in which state and input trajectories are parameterized by retractions, preserving manifold feasibility by construction without imposing extrinsic constraints.
- We propose a *manifold-consistent collocation scheme*. By transporting nodal perturbations to the same tangent space, we can apply the pseudospectral method in a standard way and integrate it with SCvx.
- We demonstrate the resulting algorithm on a six-degree-of-freedom powered-landing problem with unit quaternions and unit thrust-direction vectors, show-

ing comparable optimality to an extrinsic ACCD baseline while eliminating unit-norm drift.

The remainder of this paper is organized as follows. Section 2 reviews preliminaries on Riemannian manifolds. Sections 3 and 4 formulate the problem and discuss the limitations of standard pseudospectral methods. Section 5 presents the proposed framework, which is validated via a six-degree-of-freedom landing simulation in Section 6. Section 7 concludes the paper.

## 2. PRELIMINARIES ON RIEMANNIAN MANIFOLDS

In this section, we summarize the basic geometric operators. See Lee (2012) and Boumal (2023), for details.

Let  $\mathcal{M}$  denote a smooth manifold, which locally resembles some Euclidean space  $\mathbb{R}^n$ , and  $T_x\mathcal{M}$  its tangent space at  $x \in \mathcal{M}$ , which is a vector space consisting of tangent vectors at  $x$ . Tangent bundle  $T\mathcal{M}$  is the collection of all tangent spaces.

**Directional derivative:** For a smooth map  $f : \mathcal{M} \rightarrow \mathcal{N}$ , the directional derivative along  $\eta \in T_x\mathcal{M}$  is defined by

$$Df(x)[\eta] := \frac{d}{dt} f(\gamma(t)) \Big|_{t=0}, \quad \gamma(0) = x, \quad \dot{\gamma}(0) = \eta. \quad (1)$$

**Retraction:** A retraction is a smooth map  $R_x : T_x\mathcal{M} \rightarrow \mathcal{M}$  satisfying

$$R_x(0_x) = x, \quad DR_x(0_x) = \text{id}_{T_x\mathcal{M}}. \quad (2)$$

By this retraction, a neighborhood of  $x \in \mathcal{M}$  is parameterized by tangent vectors  $\eta \in T_x\mathcal{M}$  as

$$\gamma(t) = R_x(t\eta) \in \mathcal{M}, \text{ such that } (\gamma(0), \dot{\gamma}(0)) = (x, \eta). \quad (3)$$

When  $\mathcal{M} = \mathbb{R}^n$ , the retraction is simply  $R_x(\eta) = x + \eta$ . Other examples of retractions on the unit quaternion manifold  $\mathcal{Q}$  and the unit sphere  $S^2$  are as follows.

$$R_q(v) = q \otimes \text{Exp}(\phi), \quad \text{Exp}(\phi) = \begin{bmatrix} \cos \|\phi\| \\ \text{sinc}(\|\phi\|) \phi \end{bmatrix}, \quad (4)$$

$$R_s(w) = s \cos \|w\| + w \text{sinc}\|w\|, \quad (5)$$

where  $q \in \mathcal{Q}$ ,  $\phi \in \mathbb{R}^3$ ,  $s \in S^2$ ,  $w \in T_s S^2$ ,  $v = q \otimes \phi \in T_q \mathcal{Q}$  and  $\text{sinc}(x) := \sin x / x$ . The symbol  $\otimes$  denotes the quaternion multiplication.

**Vector transport:** A vector transport  $\mathcal{T}_{x \rightarrow y} : T_x\mathcal{M} \rightarrow T_y\mathcal{M}$  is used to compare tangent vectors based at different points. Given a retraction  $y = R_x(\eta)$ , the retraction-induced transport is defined by

$$\mathcal{T}_{x \rightarrow y}(\delta\eta) := DR_x(\eta)[\delta\eta] \in T_y\mathcal{M}, \quad (6)$$

which satisfies  $\mathcal{T}_{x \rightarrow x} = \text{id}$ . This map serves as a computationally efficient first-order approximation of parallel transport, avoiding the integration of differential equations.

**Covariant time derivative:** For a curve  $x(t) \in \mathcal{M}$  and a tangent vector field  $\eta(t) \in T_{x(t)}\mathcal{M}$  along the curve,  $D\eta/dt$  represents the covariant derivative along  $x(t)$ , which gives an intrinsic notion of time variation for vectors in moving tangent spaces. Unless otherwise stated,  $D\eta/dt$  denotes the covariant derivative along  $x(t)$  induced by the Levi-Civita connection of the Riemannian metric on  $\mathcal{M}$ .

## 3. PROBLEM STATEMENT

We address the following optimal control problem:

$$\min_{x,u} \quad J = \phi(x(t_f)) + \int_0^{t_f} L(x(t), u(t)) dt \quad (7a)$$

$$\text{s.t.} \quad \dot{x}(t) = f(x(t), u(t)), \quad x(t) \in \mathcal{M}, \quad u(t) \in \mathcal{U}, \quad (7b)$$

$$g(x(t), u(t)) \leq 0, \quad (7c)$$

$$\psi(x(0), x(t_f)) = 0, \quad (7d)$$

where  $\mathcal{M}$  and  $\mathcal{U}$  are Riemannian manifolds. Equations (7b), (7c), and (7d) represent the system dynamics, path constraints, and boundary conditions, respectively.

The objective of this paper is to develop an *intrinsic* numerical scheme for (7), inspired by intrinsic SCvx, Kraisler et al. (2025). We combine a pseudospectral transcription with successive convexification while respecting the geometry of  $\mathcal{M}$  and  $\mathcal{U}$ .

## 4. CLASSICAL PSEUDOSPECTRAL METHOD AND ITS LIMITATIONS

### 4.1 Standard Pseudospectral Method

We first review a standard pseudospectral method in a Euclidean space and then summarize its multi-segment (*hp* method) extension. The pseudospectral method is used in optimal control problems, owing to its properties as mentioned by Ross and Karpenko (2012): 1) spectral convergence, and 2) mitigation of the Runge's phenomenon.

Let  $\tau \in [-1, 1]$  denote the normalized time. Furthermore, let  $\{\tau_i\}_{i=0}^p$  be the flipped Radau nodes with  $\tau_0 = -1$  following Garg et al. (2011). The state and control are approximated using the Lagrange polynomials  $\mathcal{L}_k(\tau)$  as:

$$x(\tau) \approx \sum_{0 \leq k \leq p} x_k \mathcal{L}_k(\tau), \quad u(\tau) \approx \sum_{0 \leq k \leq p} u_k \mathcal{L}_k(\tau), \quad (8)$$

where  $x_k := x(\tau_k)$  and  $u_k := u(\tau_k)$ . Equation (8) yields the collocation dynamics, for  $i = 1, \dots, p$ ,

$$\sum_{0 \leq j \leq p} D_{ij} x_j = \sigma f(x_i, u_i), \quad \sigma := \frac{t_f - t_0}{2}. \quad (9)$$

where  $D_{ij} = \mathcal{L}'_j(\tau_i)$  represent the entries of the differentiation matrix, and  $\sigma$  serves the time-scaling factor that maps  $\tau \in [-1, 1]$  to  $t \in [t_0, t_f]$ .

The *hp*-method partitions the time horizon  $[t_0, t_f]$  into  $N$  segments. Within each segment  $h$ , the collocation constraints (9) are imposed. In this work, we assume uniform segmentation, yielding a constant time-scaling factor  $\sigma = (t_f - t_0)/(2N)$ . State continuity between adjacent segments is enforced by the linking condition  $x_p^h = x_0^{h+1}$  for  $h = 1, \dots, N-1$ .

### 4.2 Successive Pseudospectral Convexification

The pseudospectral transcription yields a finite-dimensional nonlinear program (NLP) with decision variables  $\mathbf{x} := \{x_i^h\}_{i \in [1,p]}^{h \in [1,N]}$ ,  $\mathbf{u} := \{u_i^h\}_{i \in [0,p]}^{h \in [1,N]}$ , and optionally  $\sigma$ . Using the quadrature weights  $w_i$ , the integral cost (7a) is expressed by

$$J = \phi(x_p^N) + \sigma \sum_{1 \leq h \leq N} \sum_{1 \leq i \leq p} w_i L(x_i^h, u_i^h). \quad (10)$$

Other constraints (7b)–(7d) and linking condition are transcribed as

$$\sum_{0 \leq j \leq p} D_{ij}^h x_j^h = \sigma f(x_i^h, u_i^h), \quad h=1, \dots, N \quad (11a)$$

$$g(x_i^h, u_i^h) \leq 0, \quad h=1, \dots, N \quad (11b)$$

$$\psi(x_0^1, x_p^N) = 0, \quad (11c)$$

$$x_p^h = x_0^{h+1}, \quad h=1, \dots, N-1. \quad (11d)$$

This NLP is generally nonconvex due to the nonlinear dynamics and constraints. Sagliano et al. (2021) proposes a successive convexification approach to solve this NLP efficiently. At each iteration, successive convexification linearizes nonconvex constraints about a reference  $(\bar{x}_i^h, \bar{u}_i^h, \bar{\sigma})$ . Let  $\Delta\sigma := \sigma - \bar{\sigma}$ , and let  $A_i^h$  and  $B_i^h$  denote the Jacobians of  $f$  with respect to  $x$  and  $u$ , evaluated at  $(\bar{x}_i^h, \bar{u}_i^h)$ . Then, for all collocation points  $x_i^h$ ,  $i=1, \dots, p$ ,  $h=1, \dots, N$ ,

$$\sum_{0 \leq j \leq p} D_{ij} x_j^h = \bar{\sigma}(f_i^h + A_i^h \Delta x_i^h + B_i^h \Delta u_i^h) + f_i^h \Delta\sigma, \quad (12)$$

where  $f_i^h := f(\bar{x}_i^h, \bar{u}_i^h)$ ,  $\Delta x_i^h := x_i^h - \bar{x}_i^h$ , and  $\Delta u_i^h := u_i^h - \bar{u}_i^h$ . The path constraints are linearized similarly, and the resulting convex subproblem is solved iteratively.

#### 4.3 Geometric Inconsistency on Manifolds

While the classical transcription works well in Euclidean spaces  $\mathbb{R}^n$ , its direct use becomes geometrically inconsistent when the state or control is constrained to a nonlinear manifold. The main issues of (12) are as follows:

- **Violation of state feasibility:** A polynomial interpolant is built by weighted sums in the ambient space; hence  $\sum_k x_k \mathcal{L}_k(\tau)$  is not guaranteed to lie on  $\mathcal{M}$  even if all  $x_k \in \mathcal{M}$ .
- **Mismatch of vector spaces in the dynamics:**  $\sum_j D_{ij} x_j$  is an element of  $\mathbb{R}^n$ , whereas the vector field satisfies  $f(x_i, u_i) \in T_{x_i} \mathcal{M}$ . These objects live in different spaces unless one explicitly projects or transports them.
- **Ill-posed increments for linearization:** The increment  $x_i - \bar{x}_i$  is not an intrinsic object on  $\mathcal{M}$ . Moreover, even if  $f$  is linearized in the ambient space  $f(\bar{x}, \bar{u}) + A(x - \bar{x}) + B(u - \bar{u})$  is not guaranteed to lie in the appropriate tangent space.

Existing extrinsic approaches, such as Sagliano et al. (2024), attempted to guarantee geometric consistency extrinsically, by imposing additional constraints or introducing auxiliary variables. In contrast, this paper develops an *intrinsic* scheme that strictly respects the geometry of  $\mathcal{M}$  and  $\mathcal{U}$ .

## 5. INTRINSIC SUCCESSIVE PSEUDOSPECTRAL CONVEXIFICATION

To resolve the geometric inconsistencies, the problem is formulated on the tangent bundle. Since tangent spaces admit vector-space operations, classical pseudospectral methods become directly applicable. Parameterizing the state as a perturbation from a reference trajectory and applying convexification yield the proposed intrinsic successive pseudospectral convexification scheme. Figure 1 illustrates the overall concept.

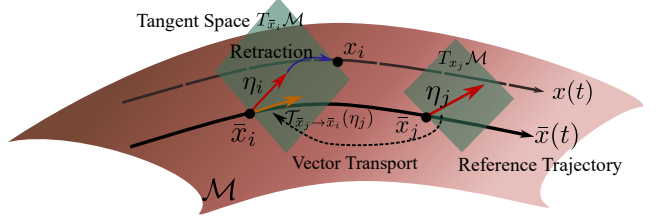


Fig. 1. Concept of intrinsic pseudospectral method. The trajectories are parameterized by retraction maps, and the perturbation dynamics are defined on the tangent bundle.

#### 5.1 Perturbation Dynamics on Tangent Bundle

Given a reference trajectory  $(\bar{x}(t), \bar{u}(t)) \in \mathcal{M} \times \mathcal{U}$ , nearby trajectories  $(x(t), u(t))$  are parameterized via retraction maps  $R$  as:

$$x(t) = R_{\bar{x}(t)}(\eta(t)), \quad \eta(t) \in T_{\bar{x}(t)} \mathcal{M}, \quad (13a)$$

$$u(t) = R_{\bar{u}(t)}(\xi(t)), \quad \xi(t) \in T_{\bar{u}(t)} \mathcal{U}. \quad (13b)$$

Since  $\eta(t)$  resides in the time-varying tangent space  $T_{\bar{x}(t)} \mathcal{M}$ , its rate of change is characterized by the covariant derivative  $D\eta/dt$ . Time-differentiation of (13) yields the velocity expansion:

$$\dot{x}(t) = D_1 R_{\bar{x}(t)}(\eta(t))[\dot{\bar{x}}(t)] + D_2 R_{\bar{x}(t)}(\eta(t)) \left[ \frac{D\eta}{dt} \right], \quad (14)$$

where  $D_1 R$  and  $D_2 R$  denote the partial derivatives of  $R_x(\eta)$  with respect to the base point  $x$  and the tangent vector  $\eta$ , respectively. Substituting  $\dot{x}(t) = f(x(t), u(t))$  into (14) gives the perturbation dynamics on  $T\mathcal{M}$ :

$$\begin{aligned} \frac{D\eta}{dt} &= \mathcal{F}(\eta, \xi) \\ &:= (D_2 R_{\bar{x}}(\eta))^{-1} \left[ f(R_{\bar{x}}(\eta), R_{\bar{u}}(\xi)) - D_1 R_{\bar{x}}(\eta)[\dot{\bar{x}}] \right]. \end{aligned} \quad (15)$$

Here  $D_2 R_{\bar{x}}(\eta)$  is assumed to be invertible in a neighborhood of  $0_{\bar{x}}$ . This holds locally since  $D_2 R_{\bar{x}}(0) = \text{Id}$  by (2).

#### 5.2 Discretization and Linearization of Dynamics and Constraints

Equation (15) is transcribed by an *hp*-pseudospectral scheme and linearized analogously to Section 4.1. Since  $\eta_k^h \in T_{\bar{x}_k^h} \mathcal{M}$  live in different tangent spaces, interpolation is formed after transporting nodal perturbations by the retraction-induced vector transport  $\mathcal{T}$ . On each segment  $h$ ,  $\eta^h(\tau)$  is approximated by

$$\eta^h(\tau) \approx \sum_{0 \leq k \leq p} \mathcal{T}_{\bar{x}_k^h \rightarrow \bar{x}^h(\tau)}(\eta_k^h) \mathcal{L}_k(\tau). \quad (16)$$

Taking the covariant derivative and evaluating at  $t = t_i$  yields

$$\left. \frac{D\eta^h}{dt} \right|_{t_i} = \frac{1}{\sigma} \sum_{0 \leq k \leq p} D_{ik} \mathcal{T}_{\bar{x}_k^h \rightarrow \bar{x}_i^h}(\eta_k^h) + \mathcal{E}_i^h(\eta_i^h), \quad (17)$$

where  $\mathcal{E}_i^h$  is the linear correction term due to the time-variation of the transport:

$$\mathcal{E}_i^h(\eta_i^h) := \left. \frac{D}{dt} \mathcal{T}_{\bar{x}_i^h \rightarrow \bar{x}^h(t)}(\eta_i^h) \right|_{t_i}. \quad (18)$$

Substituting (17) into (15) gives the equations on  $T_{\bar{x}_i^h} \mathcal{M}$ :

$$\sum_{0 \leq k \leq p} D_{ik} \mathcal{T}_{\bar{x}_k^h \rightarrow \bar{x}_i^h}(\eta_k^h) = \sigma(\mathcal{F}(\eta_i^h, \xi_i^h) - \mathcal{E}_i^h(\eta_i^h)). \quad (19)$$

Note that the left-hand side of (19) is a linear map with respect to  $\{\eta_i^h\}_{i=0}^p$ . Then the right-hand side is linearized about  $(\eta, \xi, \sigma) = (0, 0, \bar{\sigma})$ , which gives

$$\begin{aligned} \sum_{0 \leq k \leq p} D_{ik} \mathcal{T}_{\bar{x}_k^h \rightarrow \bar{x}_i^h}(\eta_k^h) &= \bar{\sigma} \left( \rho_i^h + \tilde{A}_i^h(\eta_i^h) + B_i^h(\xi_i^h) \right) \\ &\quad + \rho_i^h \Delta\sigma. \end{aligned} \quad (20)$$

Here, the operators  $\tilde{A}_i^h$ ,  $B_i^h$  are defined by

$$\tilde{A}_i^h(\cdot) := \left( D_x f(\bar{x}_i^h, \bar{u}_i^h) - C_i^h + S_{i, \rho_i^h}^h - \mathcal{E}_i^h \right)(\cdot), \quad (21a)$$

$$B_i^h(\cdot) := D_u f(\bar{x}_i^h, \bar{u}_i^h)(\cdot), \quad (21b)$$

$$C_i^h(\cdot) := D_\eta \left( D_1 R_{\bar{x}_i^h}(\eta) [\dot{\bar{x}}_i^h] \right) \Big|_{\eta=0}(\cdot), \quad (21c)$$

$$S_{i, \rho_i^h}^h(\cdot) := \left( D_\eta \left( (D_2 R_{\bar{x}_i^h}(\eta))^{-1} \right) \Big|_{\eta=0}(\cdot) \right) (\rho_i^h). \quad (21d)$$

In (21),  $D_x$ ,  $D_u$ , and  $D_\eta$  denote partial differentials with respect to the state, control, and tangent perturbation, respectively. The term  $\rho_i^h$  represents the reference defect and reference velocity  $\dot{\bar{x}}_i^h$  is given by

$$\rho_i^h := f(\bar{x}_i^h, \bar{u}_i^h) - \dot{\bar{x}}_i^h, \quad \dot{\bar{x}}_i^h \approx \frac{1}{\bar{\sigma}} \sum_{0 \leq k \leq p} D_{ik} R_{\bar{x}_i^h}^{-1}(\bar{x}_k^h), \quad (22)$$

where  $R_{\bar{x}_i^h}^{-1}(\cdot)$  is the inverse retraction map.

Nonconvex path constraints  $g(x, u) \leq 0$  are also linearized using retraction as

$$g(\bar{x}_i^h, \bar{u}_i^h) + G_i^{x, h}(\eta_i^h) + G_i^{u, h}(\xi_i^h) \leq 0, \quad (23)$$

where  $G_{x, i}^h := D_x g(\bar{x}_i^h, \bar{u}_i^h)$  and  $G_{u, i}^h := D_u g(\bar{x}_i^h, \bar{u}_i^h)$ .

### 5.3 hp-method from a Geometric Perspective

As discussed in Section 4.1, the *hp*-method divides the time horizon into multiple segments and connects states by linking conditions. From a geometric viewpoint, the *hp*-method promotes locality. Within each short segment, the reference nodes are closer, so the retraction-induced transports  $\mathcal{T}_{\bar{x}_k^h \rightarrow \bar{x}_i^h}$  tend to remain near the identity and the discrete operator  $\sum_k D_{ik} \mathcal{T}_{\bar{x}_k^h \rightarrow \bar{x}_i^h}(\eta_k^h)$  is less sensitive to curvature. Segmentation also helps keep iterates within a neighborhood where  $R_{\bar{x}}$  and  $D_2 R_{\bar{x}}$  are well behaved.

State continuity (11d) at segment interfaces is enforced through the retraction parameterization:

$$R_{\bar{x}_p^h}(\eta_p^h) = R_{\bar{x}_0^{h+1}}(\eta_0^{h+1}). \quad (24)$$

The reference trajectory is initialized and updated to satisfy continuity at interfaces (i.e.,  $\bar{x}_p^h = \bar{x}_0^{h+1}$ ). Under this condition, both perturbations  $\eta_p^h$  and  $\eta_0^{h+1}$  reside in the same tangent space  $T_{\bar{x}_p^h} \mathcal{M}$ . Since the retraction  $R_x(\cdot)$  is locally diffeomorphic at the origin, (24) simplifies to

$$\eta_p^h = \eta_0^{h+1}. \quad (25)$$

This linear formulation avoids the need for nonlinear equality constraints at the segment boundaries, significantly improving numerical tractability.

### 5.4 Coordinate Representation via Local Frames

To solve the convex subproblem using computer, abstract tangent-space quantities are converted into concrete coordinate representations. Following Kraisler et al. (2025), orthonormal frames  $E_i^h$  and  $F_i^h$  are introduced for the tangent spaces  $T_{\bar{x}_i^h} \mathcal{M}$  and  $T_{\bar{u}_i^h} \mathcal{U}$ , respectively. These frames map the perturbations  $\eta_i^h, \xi_i^h$  to coordinate vectors  $\hat{\eta}_i^h \in \mathbb{R}^n, \hat{\xi}_i^h \in \mathbb{R}^m$  such that  $\eta_i^h = E_i^h \hat{\eta}_i^h$  and  $\xi_i^h = F_i^h \hat{\xi}_i^h$ .

The operators and transport maps are converted into matrix forms  $[\tilde{A}]_i^h, [B]_i^h, [G^x]_i^h, [G^u]_i^h, [T]_{ik}^h$  via projection onto these frames. Similarly,  $\hat{\rho}_i^h$  denote the coordinate representations of the defect vector.

Consequently, the discretized constraints (20) and (23) are expressed in coordinates as:

$$\sum_{0 \leq k \leq p} D_{ik} [T]_{ik}^h \hat{\eta}_k^h = \bar{\sigma} (\hat{\rho}_i^h + [\tilde{A}]_i^h \hat{\eta}_i^h + [B]_i^h \hat{\xi}_i^h) + \hat{\rho}_i^h \Delta\sigma + \hat{\nu}_i^h, \quad (26)$$

$$g(\bar{z}_i^h) + [G^x]_i^h \hat{\eta}_i^h + [G^u]_i^h \hat{\xi}_i^h \leq \hat{s}_i^h, \quad (27)$$

where  $\hat{\nu}_i^h$  and  $\hat{s}_i^h$  are virtual control and slack variables added to ensure feasibility as in Kraisler et al. (2025).

Finally, to simplify the linking conditions, a consistent frame orientation is enforced at segment interfaces (i.e.,  $E_p^h = E_0^{h+1}$ ). This reduces the geometric continuity condition to a simple linear equality in  $\mathbb{R}^n$ :

$$\hat{\eta}_p^h = \hat{\eta}_0^{h+1}. \quad (28)$$

### 5.5 Formulation of the Convex Subproblem

At iteration  $\ell$ , we optimize the perturbations  $\mathcal{Z} := \{\hat{\eta}, \hat{\xi}, \Delta\sigma, \hat{\nu}, \hat{s}, r\}$  by solving the following subproblem:

$$\min_{\mathcal{Z}} J_{\text{cvx}}^{(\ell)} + \sum_{\substack{h=1, \dots, N \\ i=1, \dots, p}} w_i \left( \mu_\nu \|\hat{\nu}_i^h\|_1 + \mu_s (\hat{s}_i^h)_+ + \mu_r r_i^h \right) \quad (29a)$$

$$\begin{aligned} \text{s.t.} \quad \sum_{0 \leq k \leq p} D_{ik} [T]_{ik}^h \hat{\eta}_k^h &= \bar{\sigma} (\hat{\rho}_i^h + [\tilde{A}]_i^h \hat{\eta}_i^h + [B]_i^h \hat{\xi}_i^h) \\ &\quad + \hat{\rho}_i^h \Delta\sigma + \hat{\nu}_i^h \end{aligned} \quad (29b)$$

$$g(\bar{x}_i^h, \bar{u}_i^h) + [G^x]_i^h \hat{\eta}_i^h + [G^u]_i^h \hat{\xi}_i^h \leq \hat{s}_i^h, \quad (29c)$$

$$\hat{\eta}_p^h = \hat{\eta}_0^{h+1}, \quad (29d)$$

$$\left\| \hat{\xi}_i^h \right\|_2^2 \leq r_i^h, \quad (29e)$$

$$\psi(\hat{\eta}_0^1, \hat{\eta}_p^N) = 0. \quad (29f)$$

$(\cdot)_+$  denotes  $\max(0, \cdot)$ . Here,  $J_{\text{cvx}}^{(\ell)}$  is assumed to be a convex quadratic approximation of the trajectory cost about the reference (see Kraisler et al. (2025)). The weights  $\mu_\nu, \mu_s, \mu_r > 0$  penalize the virtual controls, constraint violations, and the trust region radius, respectively.

Constraint (29e) enforces a trust region on the control step. Since  $\mathcal{U}$  need not provide explicit bounds, the convexified subproblem may propose  $\hat{\xi}_i^h$  that leaves the neighborhood where the retraction  $R_{\bar{u}_i^h}(\xi)$  and its linearization are reliable. The step is therefore bounded by  $\|\hat{\xi}_i^h\|_2^2 \leq r_i^h$  and penalizes  $r_i^h$  in the objective to discourage overly large updates. Since  $\xi_i^h$  is expressed in an orthonormal frame  $F_i^h$  of  $T_{\bar{u}_i^h} \mathcal{U}$ , the coordinate norm equals the intrinsic Rie-

mannian norm:  $\|\xi_i^h\|_{\bar{u}_i^h} = \|\hat{\xi}_i^h\|_2$ . With a non-orthonormal basis,  $\|\xi\|_u^2 = \hat{\xi}^\top G \hat{\xi}$ ,  $G_{ab} = \langle F_a, F_b \rangle$ .

The overall procedure is summarized in Algorithm 1.

---

**Algorithm 1** Intrinsic Successive Pseudospectral Convexification

---

**Require:** Initial trajectory  $(\bar{x}^0, \bar{u}^0, \bar{\sigma}^0) \in \mathcal{M} \times \mathcal{U} \times \mathbb{R}$ , Weights  $\mu_\nu, \mu_s, \mu_r > 0$ , convergence tolerance  $\varepsilon > 0$ .

1:  $k \leftarrow 0$

2: **repeat**

3:   **Matrices Calculation:**

Compute  $[\bar{A}], [B], [G^x], [G^u]$ , and  $[T]$  from reference trajectory  $(\bar{x}^k, \bar{u}^k, \bar{\sigma}^k)$ .

4:   **Convex Optimization:**

Solve the convex subproblem : (29)

6:   Let  $(\hat{\eta}^*, \hat{\xi}^*, \Delta\sigma^*)$  be the optimal solution.

7:   **Update:**

8:    $\bar{x}_i^{k+1} \leftarrow R_{\bar{x}_i^k}(E_i \hat{\eta}_i^*), \bar{u}_i^{k+1} \leftarrow R_{\bar{u}_i^k}(F_i \hat{\xi}_i^*), \forall i$

9:    $\bar{\sigma}^{k+1} \leftarrow \bar{\sigma}^k + \Delta\sigma^*$

10:    $k \leftarrow k + 1$

11: **until**  $\|\hat{\eta}^*\| < \varepsilon$

**return**  $(\bar{x}^*, \bar{u}^*, \bar{\sigma}^*)$

---

## 6. NUMERICAL EXAMPLE: SIX DEGREE OF FREEDOM LANDING GUIDANCE

This section demonstrates the proposed intrinsic pseudospectral convexification method on a six-degree-of-freedom rocket landing problem.

### 6.1 Problem Formulation

The problem is adopted from Sagliano et al. (2024), with fixed time  $t_f = 4$  Ut and without RCS-induced mass consumption and torques. The formulation is briefly summarized as follows:

$$\min_{T_{\text{mag}}, \mathbf{u}_{\text{dir}}} J = -m(t_f) \quad (30a)$$

$$\left. \begin{aligned} \dot{m} &= -\alpha T_{\text{mag}}, \quad \dot{\mathbf{r}} = \mathbf{v}, \\ \dot{\mathbf{v}} &= \frac{T_{\text{mag}}}{m} C_{\mathcal{IB}} \mathbf{u}_{\text{dir}} + \mathbf{g} - \frac{D}{m}, \quad \dot{\mathbf{q}} = \frac{1}{2} \mathbf{q} \otimes \boldsymbol{\omega}, \\ \dot{\boldsymbol{\omega}} &= J^{-1} (\ell_{\text{arm}} \times T_{\text{mag}} \mathbf{u}_{\text{dir}} - \boldsymbol{\omega} \times J \boldsymbol{\omega}), \end{aligned} \right\} \quad (30b)$$

$$\left. \begin{aligned} \sqrt{r_y^2 + r_z^2} &\leq r_x \cot \gamma, \quad \|\boldsymbol{\omega}\| \leq \omega_{\text{max}}, \\ T_{\text{min}} &\leq T_{\text{mag}} \leq T_{\text{max}}, \quad m(t_f) \geq m_{\text{dry}}, \end{aligned} \right\} \quad (30c)$$

$$u_{\text{dir},1} \geq \cos \delta_{\text{max}}, \quad q_y^2 + q_z^2 \leq \sin^2(\phi_{\text{max}}/2). \quad (30d)$$

The state vector  $\mathbf{x} = [m, \mathbf{r}^T, \mathbf{v}^T, \mathbf{q}^T, \boldsymbol{\omega}^T]^T$  includes mass, position, velocity, quaternion, and angular velocity. The control input  $\mathbf{u} = [T_{\text{mag}}, \mathbf{u}_{\text{dir}}^T]^T$  consists of the thrust magnitude and direction vector. The manifold components are  $\mathbf{q} \in \mathcal{Q}$  and  $\mathbf{u}_{\text{dir}} \in S^2$ , and the retractions (4) and (5) are adopted.

Constraints involving manifold variables (e.g., (30d)) are linearized using the intrinsic scheme of Section 5.2. Constraints not involving manifold variables are purely Euclidean and convex, and are therefore kept unchanged in

the convex subproblem. A trust region (29e) is imposed on the update of  $\mathbf{u}_{\text{dir}}$  to keep steps within the local neighborhood where the retraction is accurate.

All boundary conditions and constants follow Sagliano et al. (2024), except that we set the initial attitude to  $\mathbf{q}(0) = [0.7428, -0.04278, 0.03559, 0.6672]^\top$  to enable a fair comparison with an extrinsic ACCD baseline under the same boundary/parameter settings. The penalty weights are  $\mu_\nu = 10^4$ ,  $\mu_s = 10^{-1}$ ,  $\mu_r = 10^{-2}$ . We use an  $hp$  scheme with  $N = 5$  segments and  $p = 10$  flipped Radau collocations per segment.

### 6.2 Simulation Results

Figure 2 compares the extrinsic ACCD method and the proposed intrinsic method. As shown in Fig. 2a, both methods converge to essentially the same solution in terms of trajectory shape and terminal mass ( $m_f = 1.953\,98 \text{ kg}$  for ACCD and  $m_f = 1.953\,92 \text{ kg}$  for the proposed method), indicating almost identical optimality. In contrast, Figs. 2b–2c highlight a key difference in geometric consistency. ACCD exhibits unit-norm drift (up to  $10^{-6}$ ), whereas the proposed method preserves  $\|\mathbf{q}\| = 1$  and  $\|\mathbf{u}_{\text{dir}}\| = 1$  by construction, remaining at the level of machine precision ( $\sim 10^{-15}$ ). This result is gained without renormalization or additional manifold-embedding constraints.

## 7. CONCLUSION

This paper introduced an intrinsic successive pseudospectral convexification method that bridges pseudospectral transcription and intrinsic SCvx for manifold-constrained optimal control. By expressing dynamics and increments intrinsically in local tangent spaces and coupling them with retraction-induced transports, the proposed transcription preserves manifold feasibility by construction and removes the need for extrinsic manifold constraints or auxiliary variables typically used in classical formulations. A six-degree-of-freedom powered-landing example with unit-quaternions and thrust direction vectors demonstrated comparable optimality and improved feasibility.

Future work will quantify the computational trade-off between reduced decision variables and additional geometric operations (e.g., retractions and transports), and extend the implementation to broader classes of manifolds beyond those with closed-form operators.

### DECLARATION OF GENERATIVE AI AND AI-ASSISTED TECHNOLOGIES IN THE WRITING PROCESS

During the preparation of this work the authors used chatGPT in order to assist with English proofreading and code generation assistance. After using this service, the authors reviewed and edited the content as needed and take full responsibility for the content of the publication.

## REFERENCES

Bordalba, R., Schoels, T., Ros, L., Porta, J.M., and Diehl, M. (2023). Direct collocation methods for trajectory optimization in constrained robotic systems. *IEEE Transactions on Robotics*, 39(1), 183–202.

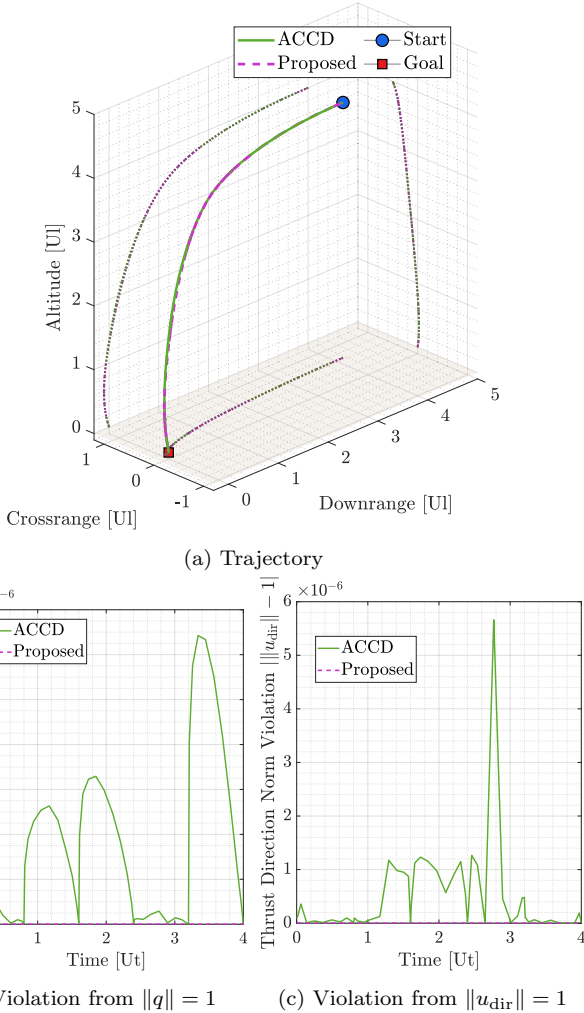


Fig. 2. Results comparison between the extrinsic ACCD method and the proposed intrinsic method. (a) Trajectories obtained by both methods. (b)(c) Unit-norm constraint violations for the quaternion  $\|q\|$  and thrust direction  $\|u_{\text{dir}}\|$  plotted on a linear scale. The proposed method stays below  $10^{-15}$ .

Boumal, N. (2023). *An introduction to optimization on smooth manifolds*. Cambridge University Press.

Garg, D., Patterson, M., Francolin, C., Darby, C., Huntington, G., Hager, W., and Rao, A. (2011). Direct trajectory optimization and costate estimation of general optimal control problems using a radau pseudospectral method. *Computational Optimization and Applications*, 49, 335–358.

Kraisler, S., Mesbahi, M., and Aćikmeşe, B. (2025). Intrinsic successive convexification: Trajectory optimization on smooth manifolds. *IEEE Control Systems Letters*, 9, 408–413.

Lee, J.M. (2012). *Introduction to Smooth Manifolds*, volume 1. Springer-Verlag, New York, 2 edition.

Lu, P. (2021). Convex-concave decomposition of nonlinear equality constraints in optimal control. *Journal of Guidance, Control, and Dynamics*, 44(1), 4–14.

Mao, Y., Szmuk, M., and Aćikmeşe, B. (2016). Successive convexification of non-convex optimal control problems and its convergence properties. In *2016 IEEE 55th Conference on Decision and Control (CDC)*, 3636–3641.

Ross, I.M. and Karpenko, M. (2012). A review of pseudospectral optimal control: From theory to flight. *Annual Reviews in Control*, 36(2), 182–197.

Saccon, A., Hauser, J., and Aguiar, A.P. (2013). Optimal control on lie groups: The projection operator approach. *IEEE Transactions on Automatic Control*, 58(9), 2230–2245.

Sagliano, M., Heidecker, A., Hernández, J.M., Farì, S., Schlotterer, M., Woicke, S., Seelbinder, D., and Dumont, E. (2021). Onboard guidance for reusable rockets: Aerodynamic descent and powered landing. In *AIAA Scitech 2021 Forum*.

Sagliano, M., Seelbinder, D., Theil, S., and Lu, P. (2024). Six-degree-of-freedom rocket landing optimization via augmented convex-concave decomposition. *Journal of Guidance, Control, and Dynamics*, 47(1), 20–35.

Szmuk, M. and Aćikmeşe, B. (2018). Successive convexification for 6-dof mars rocket powered landing with free-final-time. In *2018 AIAA Guidance, Navigation, and Control Conference*.

Szmuk, M., Reynolds, T.P., and Aćikmeşe, B. (2020). Successive convexification for real-time six-degree-of-freedom powered descent guidance with state-triggered constraints. *Journal of Guidance, Control, and Dynamics*, 43(8), 1399–1413.

## Appendix A. QUATERNION RETRACTION: CLOSED-FORM TERMS AND TRANSPORTS

In this appendix, the closed-form expressions of the retraction-induced terms used in Section 6 are summarized for the unit-quaternion manifold  $\mathcal{Q}$ . All expressions below are given in the minimal coordinates  $v \in \mathbb{R}^3$ . Let  $J_r(\phi) \in \mathbb{R}^{3 \times 3}$  denote the right Jacobian, with the standard expansion  $J_r(\phi) \approx I - 1/2[\phi]_x + 1/6[\phi]_x^2$  for  $\|\phi\| \approx 0$ , where  $[\cdot]_x$  is the skew-symmetric matrix operator.

### A.1 Closed-form of $C$ , $S$ , and $\mathcal{E}$

For the quaternion kinematics  $\dot{q} = 1/2 q \otimes \omega_B$  and a reference  $(\bar{q}, \bar{\omega}_B)$ , the retraction-induced terms in (21) satisfy

$$[C_i^q] = 0, \quad [S_{i,\rho_i^q}]v = [\rho_i^q]_x v, \quad [\mathcal{E}_i^q]v = [\bar{\omega}_{B,i}]_x v, \quad (\text{A.1})$$

where  $\rho_i^q \in \mathbb{R}^3$  is the defect expressed in the same minimal coordinates.

### A.2 Closed-form of the transport matrices $[T]_{ik}^h$

In the numerical example,  $\mathcal{M}$  is a product of Euclidean components and  $\mathcal{Q}$ , so  $[T]_{ik}^h$  is block-diagonal. The Euclidean block is  $I$ . The quaternion block is given by  $J_r(\phi)$ , so  $[T]_{ik}^h$  satisfies

$$[T]_{ik}^h = \text{diag}(I, J_r(\phi_{ki}^h)), \quad (\text{A.2})$$

$$J_r(\phi) = I_3 - \frac{1 - \cos \theta}{\theta^2} [\phi]_x + \frac{\theta - \sin \theta}{\theta^3} [\phi]_x^2. \quad (\text{A.3})$$

$$\phi_{ki}^h := 2 \text{Log}((\bar{q}_k^h)^{-1} \otimes \bar{q}_i^h) \in \mathbb{R}^3, \quad (\text{A.4})$$

where  $\theta = \|\phi\|$ .